

Three-dimensional modes in a periodically driven elongated cavity

Jonathan J. F. Leung and Amir H. Hirsra

Department of Mechanical, Aerospace and Nuclear Engineering, Rensselaer Polytechnic Institute, Troy, New York 12180, USA

Hugh M. Blackburn

CSIRO Manufacturing and Infrastructure Technology, P. O. Box 56, Highett, Victoria 3190, Australia

Francisco Marques

Departament de Física Aplicada, Universitat Politècnica de Catalunya, 08034 Barcelona, Spain

Juan M. Lopez

Department of Mathematics and Statistics, Arizona State University, Tempe, Arizona 85287, USA

(Received 12 July 2004; revised manuscript received 5 November 2004; published 11 February 2005)

Three-dimensional instability modes of the periodic flow in a rectangular cavity driven by the harmonic sliding oscillation of its floor are explored experimentally. Theory for a cavity with infinite span predicts two synchronous modes and a quasiperiodic traveling-wave mode as primary transitions from two-dimensional to three-dimensional flow for different combinations of floor oscillation amplitude and frequency. Previously, only one of the two synchronous modes had been found experimentally. Here, we provide experimental details of both synchronous modes and a quasiperiodic mode. All three modes appear in the parameter regimes predicted by the theory; however, in the finite-span experiments, the traveling wave nature of the quasiperiodic mode is replaced by a nonpropagating mode with spatial features similar to those of the traveling mode.

DOI: 10.1103/PhysRevE.71.026305

PACS number(s): 47.15.Fe, 47.20.-k, 47.20.Ky, 47.54.+r

I. INTRODUCTION

The transition from two-dimensional to three-dimensional flow is of fundamental interest in fluid dynamics. For time-periodic two-dimensional flows with spatiotemporal symmetries, three distinct generic primary instabilities have recently been described and analyzed theoretically [1]. For the most part, numerical and experimental attention has focused solely on synchronous modes that either break or preserve the spatiotemporal symmetry, e.g., in bluff body wake flows [2–6]. Recent computations on wake flows, however, indicate that a quasiperiodic mode can also be the primary mode in the two-dimensional to three-dimensional transition [7].

Another flow with the same spatiotemporal symmetries as the periodically shedding wake flows is that in a periodically driven rectangular cavity of infinite spanwise extent, which was the subject of a previous numerical study [8] covering Floquet stability analysis of three-dimensional modes. In the present paper, we describe experiments in a finite-length cavity, shown schematically in Fig. 1. The flow is governed by two dynamic parameters: the Reynolds number, which characterizes the amplitude of the floor oscillation,

$$Re = V_{\max} h / \nu$$

(where V_{\max} is the peak floor velocity, h is the cavity vertical height, and ν is the kinematic viscosity of the fluid), and the Stokes number, which is the ratio of the vertical viscous diffusion time (h^2/ν) to the floor oscillation period (T),

$$St = h^2 / T\nu.$$

The two-dimensional time-periodic basic state consists of the boundary layer on the oscillating floor rolling up to form

a two-dimensional vortex (“roller”) at one end of the cavity with each stroke of the floor. For low St , the roller at one end dissipates while the floor stroke is reversed and another roller forms at the other end. In contrast, for large St , the counter-rotating rollers at each end persist throughout the entire floor oscillation period, which is now short compared to the vis-

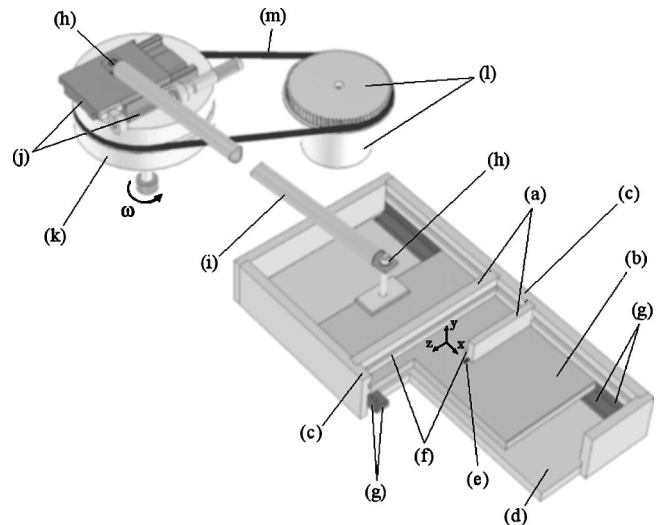


FIG. 1. Schematic of experimental apparatus and coordinate system. The letters indicate (a) sidewalls at $x = \pm\Gamma/2$; (b) oscillatory glass floor; (c) end walls at $z = \pm\Lambda/2$; (d) floor of the acrylic container; (e) dynamic seals; (f) free-surface groove and solid wall position at $y=h$; (g) Teflon slide pads for oscillatory glass floor; (h) ball bearings; (i) connecting rod; (j) linear translation stage and micrometer; (k) drive wheel; (l) belt pulley and stepper motor; (m) drive belt.

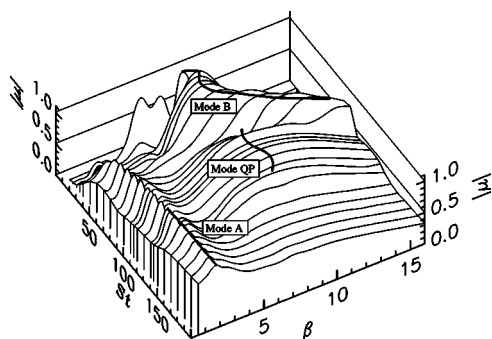


FIG. 2. Variation of the modulus of the most dangerous Floquet multiplier $|\mu|$ with spanwise wave number β over a range $St \in [10, 200]$ at the critical Re for each value of St for the infinite-span cavity [8]. The three thick lines are the loci $|\mu|=1$ for each of the three modes.

cous diffusion time. These differences in the characteristics of the basic state for different St are responsible for the distinct primary modes of instability to three-dimensional flow as St is varied.

In the infinite-span systems, the base-state velocity at any location is the same as that obtained by a $T/2$ evolution in time and a reflection in $x=0$ (a “half-period flip”). The action of this spatiotemporal symmetry H on the vorticity $(\xi, \eta, \zeta) = \nabla \times (u, v, w)$ is

$$H(\xi, \eta, \zeta)(x, y, z, t) = (\xi, -\eta, -\zeta)(-x, y, z, t + T/2). \quad (1)$$

Our experimental results concentrate on the properties of the vertical component of vorticity, η . In infinite-span systems, the basic state is also spanwise (z) invariant at all times.

The only three-dimensional state bifurcating from the basic state that had been previously observed experimentally, in a finite span cavity, was an H -symmetric synchronous (T -periodic) mode (mode B) [9]. Subsequently, Floquet analysis [8] predicted the presence of a further synchronous mode (mode A), as well as a quasiperiodic mode (mode QP); the latter manifesting itself as a modulated spanwise-traveling wave (TW). These theoretical results are summarized in Fig. 2, which shows the modulus of the most dangerous Floquet multiplier $|\mu|$ as a function of spanwise wave number $\beta=2\pi h/\lambda$, and of St , at the corresponding critical Re for each of these modes.

The structures of the three modes A , B , and TW in the infinite-span cavity are illustrated by instantaneous vorticity isosurfaces in Fig. 3, obtained via direct numerical simulation (DNS) [8]. By comparing the signs of η at times $T/2$ apart with Eq. (1), it can be seen that mode A breaks H symmetry and mode B preserves it. Mode TW has no symmetry in a fixed reference frame, but in a frame moving at phase velocity, the wave has H symmetry. The phase velocity is related directly to T_s/T , where T_s is the new secondary period arising at the bifurcation to quasiperiodicity. Figure 4 shows the values of this ratio predicted by Floquet analysis.

In the finite-span case, the system retains the spatiotemporal symmetry H , but the spanwise end walls destroy the translation invariance in the spanwise direction, leaving only the spatial reflection about the midspan. Effects of replacing

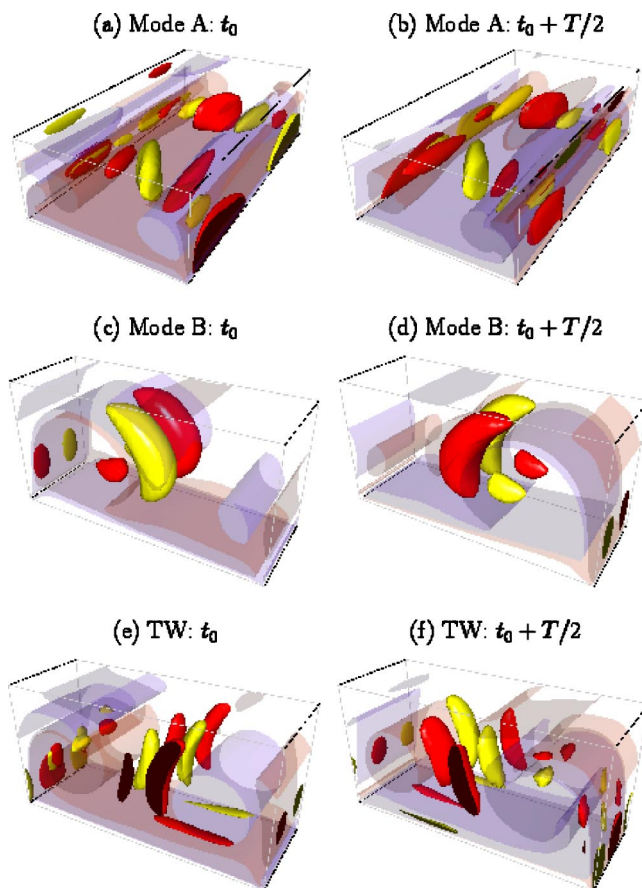


FIG. 3. (Color online) Isosurfaces of the vertical (solid) and spanwise (translucent) components of vorticity (i.e., η and ζ) from DNS [8], for (a),(b) mode A at $Re=1250$, $St=160$, and $\beta=1.7$, (c),(d) mode B at $Re=535$, $St=20$, and $\beta=8.75$, and (e),(f) quasi-periodic TW at $Re=1225$, $St=100$, and $\beta=8.5$, each at two times $T/2$ apart.

a translation (continuous) symmetry by a reflection (discrete) symmetry in fluid dynamics have been extensively studied [10], and particularly so in the Taylor-Couette problem. When the instability of the basic state is stationary, it has been observed that the large- (but finite-) aspect-ratio limit is very different from the idealization of an infinite direction

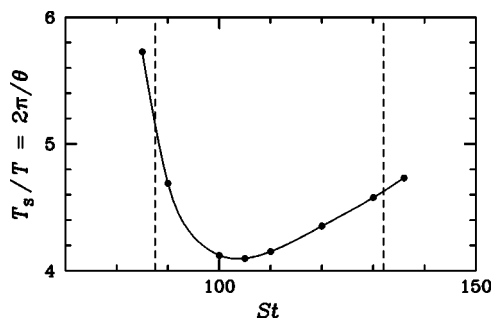


FIG. 4. Predicted secondary periods $T_s/T=2\pi/\theta$ of the quasiperiodic mode QP, where $\exp \pm i\theta$ are the critical Floquet multipliers at the Neimark-Sacker bifurcation [8]. Mode QP is the primary mode of instability from the basic state for St values between the vertical dashed lines.

[11–14]. When the instability is via a Hopf bifurcation, the effects of end walls that break the translation invariance in large-aspect-ratio systems has been considered as an imperfection problem [15], and recent experiments in Taylor-Couette flow are in agreement with many details of the theory [16,17]. However, these studies have only considered autonomous systems with purely spatial symmetries. For our nonautonomous problem, with the space-time symmetry H , no theory has yet been developed to account for finite-aspect-ratio effects.

The main objectives of the present study are to determine experimentally if the predicted synchronous mode A and quasiperiodic mode QP can be obtained in the finite-length cavity, and show how the presence of end walls might affect the traveling-wave nature predicted for mode QP .

II. EXPERIMENTAL APPARATUS AND TECHNIQUE

The apparatus (see Fig. 1) has been described in detail in [9]. Only the salient features of its design and the modifications that were necessary for the present experiment are described here.

The frame of the oscillatory driven cavity was machined to a precision of $\pm 30 \mu\text{m}$ from cast acrylic plates, and except for the parts that had to be made removable for disassembly and cleaning, the pieces were permanently joined by solvent bonding. The acrylic frame functions as spanwise end walls of the cavity, and the cavity sidewalls are retained by the frame. The oscillatory driven floor of the cavity, made of optical quality glass, was supported by Teflon slide pads within the frame. The top wall of the cavity was made of glass, which was fitted inside grooves machined into the sidewalls. The height, width, and span of the cavity were $h = 10 \text{ mm}$, $\Gamma h = 20 \text{ mm}$, and $\Lambda h = 194 \text{ mm}$, respectively.

Distilled water (nominal viscosity of $\nu = 9.57 \times 10^{-7} \text{ m}^2/\text{s}$ at 22°C) was utilized for the experiments. Flow was measured using the digital particle image velocimetry technique (DPIV; e.g., see [18]). For the measurements with DPIV, water was seeded with polystyrene particles, in the range of $20\text{--}25 \mu\text{m}$ (Duke Scientific, 7520A and 7525A), depending on the requisite field of view.

The dynamic seals, used on the bottom of the sidewalls where they contacted the oscillatory driven floor, were made of Buna-n rubber O-ring material, cut to length. Once the submerged acrylic pieces had equilibrated and swelling due to water uptake had ceased, Teflon shims ($50 \mu\text{m}$ thickness) were used as gaskets between acrylic pieces that were screwed together. The shims provided positive seals between the ends and sidewalls, and ensured a smooth motion of the oscillatory glass floor.

The oscillating floor was actuated by a drive wheel and a crank arm. The drive wheel was spun by a stepper motor through a timing belt (W. M. Berg, part number TB7UP4-380) and pulley (TP20L6U6-78). The ratio of the drive wheel diameter to the pulley diameter on the motor was approximately 1.22:1. The amplitude of the floor motion was set using a microtranslation stage, which was mounted on the drive wheel. The accuracy of the microtranslation stage in setting the floor amplitude was checked using a dial indicator

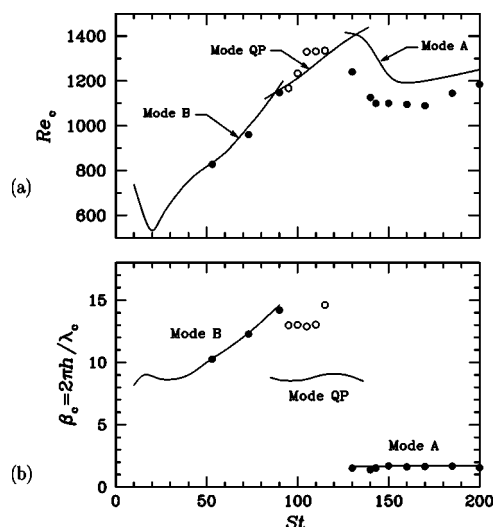


FIG. 5. Variations of (a) Re_c and (b) β_c with St ; the solid lines are determined via Floquet analysis in the limit $\Lambda \rightarrow \infty$ [8] and filled (open) symbols correspond to synchronous (quasiperiodic) experimental states in the cavity with $\Lambda = 19.4$.

(with $3 \mu\text{m}$ resolution) against the crank arm mounting post on the glass floor and found to be approximately $\pm 30 \mu\text{m}$. The water temperature within the apparatus was monitored using a platinum resistance temperature detector (probe, Omega, model PR-11-2-100-1/16-6-E, and display, Omega, model 4201A-PC2) to an accuracy of $\pm 0.1^\circ\text{C}$. For each experiment, the amplitude of the floor motion was set using the microtranslation stage so that a prescribed Reynolds number could be obtained at the given temperature and corresponding viscosity. On the other hand, only the nominal value of the Stokes number could be prescribed in each experiment due to quantization effects between the stepper motor controller and the data acquisition system. The uncertainty in determining the Reynolds number, resulting from errors in the amplitude and frequency of the floor motion, as well as the temperature dependence of viscosity, is approximately 0.27%. The uncertainty in determining the Stokes number, due to errors in viscosity and frequency, is approximately 0.23%.

III. RESULTS

Figure 5 summarizes the quantitative comparison between Floquet analysis of the infinite-span case and the current experiments with $\Lambda = 19.4$: (a) shows critical Re as a function of St , illustrating the onset of mode B for low St , mode A for large St , and mode QP for intermediate St ; (b) shows the corresponding critical wave numbers β_c . The ranges of St for the onset of each of the three modes agree quite well. The values of the critical Re for modes B and QP also agree well. However, for mode QP the observed wave numbers do not match the theoretical predictions for the infinite-span system, and the onset of mode A takes place at a lower Re than predicted. A detailed analysis of the three observed modes follows.

A. Synchronous mode A : Broken H symmetry

For mode A , the critical Re observed experimentally is approximately 10% lower than that determined via Floquet

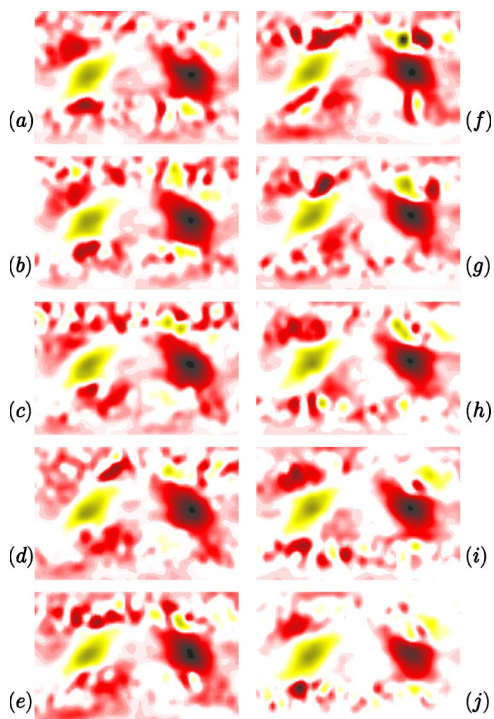


FIG. 6. (Color online) Contours of the instantaneous vertical vorticity η at mid-depth $y/h=0.5$, over $x/h \in [-\Gamma/2, \Gamma/2]$ and $z/h \in [-0.1\Lambda, 0.1\Lambda]$ for a mode A state at $Re=1300$, $St=160$ over one period $T=0.651$ s; interval between each frame is $T/10$.

analysis in the $\Lambda \rightarrow \infty$ limit [Fig. 5(a)]. We note that in the analysis [8], the onset of mode A was via a degenerate pitchfork bifurcation (borderline between super- and subcritical). The experiments suggest that the pitchfork is subcritical for $\Lambda=19.4$. Note that pitchfork bifurcations are very sensitive to small imperfections which tend to unfold them into distinct branches of solutions, one that is smoothly connected to the basic state, and another “anomalous” disconnected branch [11,19,20]. Nevertheless, the experimentally observed critical wave numbers for mode A agree very well with the Floquet results [Fig. 5(b)].

Figure 6 shows contours in the midplane ($y/h=0.5$) of the vertical component of vorticity η (determined from DPIV measurements of the horizontal components of velocity) for a mode A state at $Re=1300$ and $St=160$. The ten frames are instantaneous snapshots taken uniformly over one floor oscillation period $T=0.651$ s. The DPIV imaging window extends over approximately one spanwise wavelength ($z/h \in [-0.1\Lambda, 0.1\Lambda]$, horizontal direction in the figure) and the entire cavity width ($x/h \in [-\Gamma/2, \Gamma/2]$, toward the top and bottom of the page). One of the striking features of this figure is the near-constant presence of the large counter-rotating vortical structures in the middle of the figure. These are inter-roller secondary vortices that are continuously being “fed” by the large core deformations of the two spanwise rollers at either x end of the cavity. Their persistence over the entire forcing period is consistent with the Floquet analysis, where the mode A eigenfunctions also show such vortices. The Floquet modes are not inclined, but rather are symmetric about $x=0$. However, nonlinear solutions show the same level of

oblique inclination when viewed from the top (positive y), as is observed experimentally—see Figs. 3(a) and 3(b), which show a nonlinear mode A solution at times $T/2$ apart, where the inclined inter-roller secondary vortices and the core deformations of the primary rollers are clearly seen.

Consider now the symmetries of the experimentally observed mode A . Comparing experimentally measured η for mode A at times $T/2$ apart [e.g., comparing parts (a) and (f) of Fig. 6], it is apparent that it is not H symmetric; the light (yellow) [dark (red)] vortex in (f) should be dark (red) [light (yellow)] if it were H symmetric, according to Eq. (1). Hence the spatiotemporal symmetry of mode A in the finite cavity (as observed in the central portion of the cavity) is the same as that of the infinite-span problem.

The critical wave numbers β measured experimentally for mode A agree with Floquet analysis, but the critical Re are substantially smaller. There are a number of points to consider in reconciling this difference.

(1) The theoretical onset of mode A is degenerate (the cubic term in the normal form vanishes). This raises the question as to whether the onset in the experiment is subcritical or supercritical. The answer to this question is complicated by the fact that the experiment does not have perfect z -reflection symmetry, and so the pitchfork is unfolded.

(2) Mode A has large wavelength (small β), so quantization effects in a finite box may be important.

(3) Mode A is a large-frequency mode in which the two spanwise rollers persist throughout the whole forcing period. This means that long-term interactions between the rollers and the spanwise end walls are possible, and these interactions are simply not present in the Floquet and nonlinear numerical analyses.

In summary, the comparison between the experiments and the theory suggests that mode A is subcritical, and that it is strongly influenced by the end walls because of its large wavelength and the persistence of the primary rollers.

B. Synchronous mode B : Preserved H symmetry

Figure 7 shows instantaneous contours, from DPIV measurements, of η at the midplane $y/h=0.5$ for a mode B state at $Re=1000$ and $St=53$ over one floor oscillation period. This state is also invariant to z reflections about the z nodal points in η . It is also H symmetric; taking an image in the left column of the figure, reflecting it about $x=0$, and changing the sign of η results in an image corresponding to η at time $T/2$ later (the image in the right column, on the same row). Thus, the experimentally observed finite cavity mode B has the same spatiotemporal symmetry as mode B in the $\Lambda \rightarrow \infty$ case.

End wall effects on mode B appear to be minimal. The wavelength for mode B is very small compared with the spanwise extent of the cavity, and we find for this mode that the finite- Λ experiments behave very much like the $\Lambda \rightarrow \infty$ case. Further, mode B is a low-frequency (small- St) mode where the spanwise rollers only survive for about half the floor oscillation period; this means there is no long-term interaction between the rollers and the spanwise end walls (which is not the case for either mode A or mode QP).

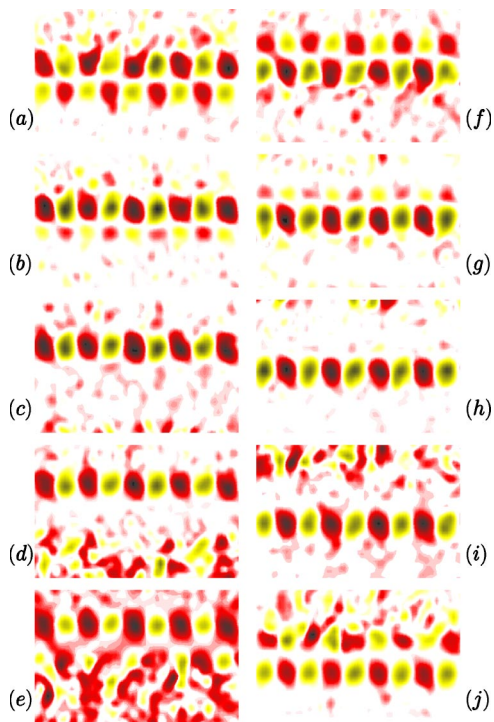


FIG. 7. (Color online) Contours of the instantaneous vertical vorticity η at mid-depth $y/h=0.5$, over $x/h \in [-\Gamma/2, \Gamma/2]$ and $z/h \in [-0.07\Lambda, 0.07\Lambda]$ for a mode B state at $Re=1000$, $St=53$ over one period $T=1.965$ s; interval between each frame is $T/10$.

Of the three modes (A , B , and QP) analyzed in this paper, only mode B has been previously observed experimentally in the finite cavity to our knowledge. This mode is described in more detail in [9].

C. Quasiperiodic mode QP: Complete symmetry breaking

For mode QP , the observed critical wave numbers differ from the Floquet values by approximately 40%. This is a large difference, but it should be noted that from the Floquet analysis, the variation of β with St is very flat for mode QP , and so there is not a clear selection of a single β for the nonlinear state (see Fig. 2).

The snapshots of the vertical vorticity η , at mid-depth over one floor oscillation period, for the experimentally observed mode QP , are shown in Fig. 8. It is seen to be organized into oblique bands of alternating positive and negative η . The band structure remains fairly constant throughout the floor oscillation period, and is only broken up for short instances, e.g., in frames (e) and (f). However, η is not constant within the bands. There is a fairly well-discernible maximum in each band, and these maxima travel back and forth along the bands in unison. It is not straightforward to find much coherence in this motion, in part because the flow is quasiperiodic. Figure 9 is a phase-averaged image, taken at the particular phase corresponding to Fig. 8(e), with averaging over 34 floor oscillation periods. Since the mode is quasiperiodic, some care needs to be taken in interpreting this image, but it serves to underscore the point that, in the finite-length cavity, this is not a spanwise traveling-wave mode.

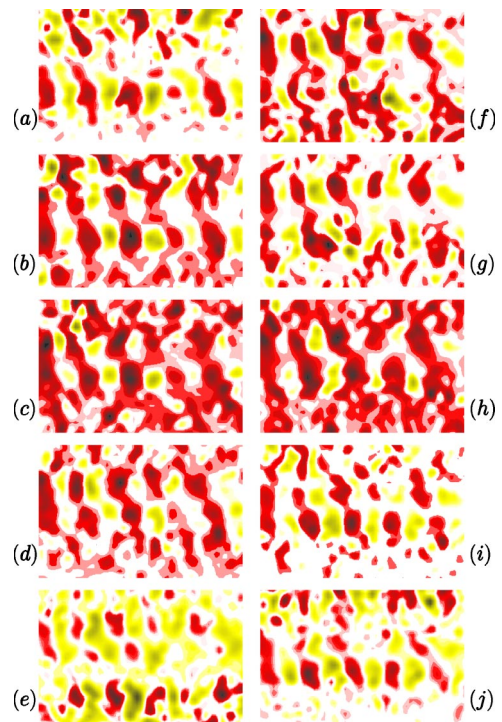


FIG. 8. (Color online) Contours of the instantaneous vertical vorticity at mid-depth $y/h=0.5$, over $x/h \in [-\Gamma/2, \Gamma/2]$ and $z/h \in [-0.07\Lambda, 0.07\Lambda]$ for a QP state at $Re=1400$, $St=105$ over one period $T=0.999$ s; interval between each frame is $T/10$.

We have observed the flow over hundreds of floor cycles and the oblique banded structure does not move in the z direction. On the other hand, the lack of spanwise reflection symmetry, also a key feature of the predicted TW mode, is clearly evident.

The quasiperiodicity of this flow is established using time series of the spanwise velocity measured via DPIV in a small region near the center of the cavity. In taking these measurements, we have strobed the flow at the floor oscillation period and recorded the z velocity at the same phase over 1024 periods. The power spectral density of this strobed velocity signal (obtained via discrete Fourier transform) is shown in Fig. 10, where a very distinct signal with period $4.61T$ is evident. We interpret this signal as being the quasiperiodic motion of the η maxima along the bands.

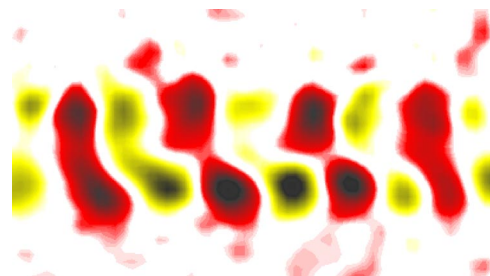


FIG. 9. (Color online) Contours of phase-averaged vertical vorticity η at mid-depth $y/h=0.5$, over $x/h \in [-\Gamma/2, \Gamma/2]$ and $z/h \in [-0.07\Lambda, 0.07\Lambda]$, for the QP state of Fig. 8.

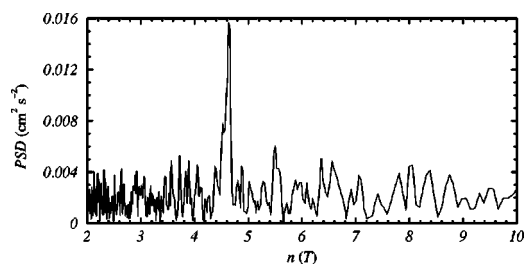


FIG. 10. Power spectral density vs period (in terms of the base period T) of the z velocity of the QP state, in a small (x, y) region of size 0.09×0.09 cm² about the point $x/h = -0.1\Gamma$, $y/h = 0.5$, $z/h = -0.03\Lambda$, for $\text{Re} = 1400$ and $\text{St} = 105$.

The secondary (modulation) period of QP seen in Fig. 10 compares well with the propagation period of the modulated traveling waves in the $\Lambda \rightarrow \infty$ case (TW), which is in the range of $4.1T$ to $4.8T$ for the values of St for which TW is the primary mode of instability. See Fig. 4 for these periods as determined via Floquet analysis.

The symmetries of QP and TW are different. They both have broken the z -reflection symmetry, and although in the central region of the cavity QP appears to be periodic in z , this is not so over the whole of the cavity owing to the presence of the spanwise end walls. We do not present DPIV data near these end walls as the unsteady three-dimensional structure of the flow in these regions significantly reduces the signal-to-noise ratio to a point where conclusive statements cannot be made. In contrast, TW, which breaks the continuous z -translation symmetry, retains a discrete z -translation symmetry corresponding to its spatial periodicity of wave number β . Recall that although TW has broken the spatiotemporal H symmetry, it retains a spatiotemporal symmetry comprised of H composed with an appropriate z translation (this translation is the distance the wave propagates in time $T/2$, applied in the opposite direction). QP does not have any (spatial or spatiotemporal) symmetry.

The relationship between QP and the quasiperiodic modes from the Floquet analysis (SW and TW) may be interpreted along similar lines as the relationship between the ribbons and spirals (standing and traveling modes, respectively) in classic counter-rotating Taylor-Couette flow (i.e., with infinite cylinders) and the corresponding modes found in finite-length systems. In the infinite case (treated as periodic in z), the spirals and ribbons arise via Hopf bifurcations in a system that is invariant to translations and reflections in the axial direction z . These standing and traveling waves bifurcate simultaneously. The spirals are traveling waves in z that break the reflection symmetry, so there are two different spirals corresponding to traveling waves in the directions $+z$ and $-z$, and the z reflection transforms one into the other. The ribbons are reflection symmetric standing waves, which break the translational symmetry, so there is a continuous family of ribbons parametrized by their phase in z [10]. In our nonautonomous system, the Hopf-like bifurcation (Neimark-Sacker bifurcation, leading to quasiperiodic behavior) also results in a pair of modulated traveling waves TW that break the reflection symmetry, and are transformed one into the other by the z reflection, and a continuous family

of modulated standing waves SW parametrized by their phase in z [1]. In the $\Lambda \rightarrow \infty$ driven cavity, SW is unstable and the TW are stable. In Taylor-Couette flow, as predicted from normal form theory [15] and observed experimentally [16,17], the Hopf bifurcation in finite-length systems results in two different types of standing waves, having either even or odd parity in z . The frequency of oscillation of these waves matches very well the Hopf frequency determined from stability analysis in the infinite case. A travelinglike mode is also found in the finite cases, but only as a secondary state bifurcating from one or other of the two standing waves (which do not bifurcate simultaneously). Although our system is different from Taylor-Couette flow, because it is periodically forced and has the additional space-time symmetry H , the strong similarities in the infinite case suggest that QP comes about via an analogous process and is a result of the presence of spanwise end walls.

IV. CONCLUSIONS

The three possible types of codimension-1 bifurcations from a (nominally) two-dimensional time-periodic basic state to three-dimensional flow, predicted from normal form theory for a strictly two-dimensional flow, have now been observed experimentally as primary bifurcations. The range of forcing frequencies (St) over which each mode is primary agrees very well with the Floquet analysis. Two of the modes are synchronous; one retains the spatiotemporal symmetry of the basic state and the other breaks it. For the symmetric synchronous mode, both the critical forcing amplitude (Re) and wavelength agree with the Floquet analysis. For the symmetry-breaking synchronous mode, the critical wavelength is in agreement but the mode bifurcates at lower Re (approx. 10% lower) than predicted by Floquet analysis. Possible reasons for this discrepancy include that the Floquet analysis shows the pitchfork bifurcation to be degenerate and so end walls may change this to a subcritical pitchfork, and also that this mode is a high frequency instability of a basic state consisting of spanwise rollers which remain coherent throughout the whole forcing cycle so that long-term interactions between these and the spanwise end walls are probable. Also, the wavelength of this mode is relatively large (only approximately four wavelengths fit in the finite cavity), further enhancing end wall effects. The third primary mode is quasiperiodic. The observed modulation frequency is close to that of the quasiperiodic mode from Floquet analysis, as is the critical Re . However, the physical manifestation of the modulation frequency is very different from that in the infinite cavity where this mode corresponds to a modulated traveling wave. In the finite cavity, this mode does not propagate in the spanwise direction. However, its spatial structure consists of braidlike structures wrapped around each of the spanwise rollers that are interlaced obliquely across the roller, just like the spatial structure of the traveling-wave mode in the infinite case.

Further investigations into end wall effects would be useful. At present, there is no theory for end wall interactions in periodically forced systems such as these. Such theoretical developments would also be of use in autonomous systems where secondary bifurcations from two-dimensional time-periodic states result in the transition to three-dimensional flows, such as is the case in many bluff body wake flows.

ACKNOWLEDGMENTS

This work was partially supported by the National Science Foundation (J.J.F.L., A.H.H., and J.M.L.), Ministry of Science and Technology (F.M.), and the Australian Academy of Science and the Australian Partnership for Advanced Computing (H.M.B.).

-
- [1] F. Marques, J. M. Lopez, and H. M. Blackburn, *Physica D* **189**, 247 (2004).
 - [2] C. H. K. Williamson, *Phys. Fluids* **31**, 3165 (1988).
 - [3] C. H. K. Williamson, *J. Fluid Mech.* **328**, 345 (1996).
 - [4] D. Barkley and R. D. Henderson, *J. Fluid Mech.* **322**, 215 (1996).
 - [5] D. Barkley, L. S. Tuckerman, and M. S. Golubitsky, *Phys. Rev. E* **61**, 5247 (2000).
 - [6] S. Julien, J. Lasheras, and J.-M. Chomaz, *J. Fluid Mech.* **479**, 155 (2003).
 - [7] H. M. Blackburn, F. Marques, and J. M. Lopez, *J. Fluid Mech.* **522**, 395 (2005).
 - [8] H. M. Blackburn and J. M. Lopez, *J. Fluid Mech.* **497**, 289 (2003).
 - [9] M. J. Vogel, A. H. Hirs, and J. M. Lopez, *J. Fluid Mech.* **478**, 197 (2003).
 - [10] J. D. Crawford and E. Knobloch, *Annu. Rev. Fluid Mech.* **23**, 341 (1991).
 - [11] T. B. Benjamin and T. Mullin, *Proc. R. Soc. London, Ser. A* **377**, 221 (1981).
 - [12] A. Lorenzen and T. Mullin, *Phys. Rev. A* **31**, 3463 (1985).
 - [13] K. A. Cliffe, J. J. Kobine, and T. Mullin, *Philos. Trans. R. Soc. London, Ser. A* **439**, 341 (1992).
 - [14] A. M. Rucklidge and A. R. Champneys, *Physica D* **191**, 282 (2004).
 - [15] A. S. Landsberg and E. Knobloch, *Phys. Rev. E* **53**, 3579 (1996).
 - [16] J. Langenberg, G. Pfister, and J. Abshagen, *Phys. Rev. E* **68**, 056308 (2003).
 - [17] J. Langenberg, G. Pfister, and J. Abshagen, *Phys. Fluids* **16**, 2757 (2004).
 - [18] A. H. Hirs, J. M. Lopez, and R. Miraghie, *J. Fluid Mech.* **443**, 271 (2001).
 - [19] T. B. Benjamin, *Proc. R. Soc. London, Ser. A* **359**, 1 (1978).
 - [20] T. B. Benjamin, *Proc. R. Soc. London, Ser. A* **359**, 27 (1978).